# Compliant Electromagnetic Actuator Architecture for Soft Robotics

Noah Kohls[1], Beatriz Dias[1], Yaw Mensah[1], Bryan P. Ruddy[2], and Yi Chen Mazumdar[1,*]

***Abstract*— Soft materials and compliant actuation concepts have generated new design and control approaches in areas from robotics to wearable devices. Despite the potential of soft robotic systems, most designs currently use hard pumps, valves, and electromagnetic actuators. In this work, we take a step towards fully soft robots by developing a new compliant electromagnetic actuator architecture using gallium-indium liquid metal conductors, as well as compliant permanent magnetic and compliant iron composites. Properties of the new materials are first characterized and then co-fabricated to create an exemplary biologically-inspired soft actuator with pulsing or grasping motions, similar to *Xenia* soft corals. As current is applied to the liquid metal coil, the compliant permanent magnetic tips on passive silicone arms are attracted or repelled. The dynamics of the robotic actuator are characterized using stochastic system identification techniques and then operated at the resonant frequency of 7 Hz to generate high-stroke (>6 mm) motions.**

## I. INTRODUCTION

Soft materials and compliant actuators have generated interesting new motions and control techniques for robots, automated systems, and wearable devices. Soft robotic systems show great promise for mimicking biological systems, altering their shape to fit into tight spaces, grasping arbitrarily-shaped objects, enhancing physical human-robot interaction, improving biological-to-electrical interfaces, and adapting to complex environments. Despite the potential of soft robotic systems, many designs currently use classical hard actuators including pumps, valves, and motors. Other soft actuation mechanisms including light-sensitive [1], heat-sensitive [2], shape-memory [3], electroactive polymer [4], [5], electrostatic [6], muscle [7], elastic [8], hydraulic [9], [10], and pneumatic [11] toplogies have also been explored [12], [13], [14]. Most of these methods rely on generating strain (bending, contraction, and extension) for motion. In contrast, efficient linear and rotary electromagnetic actuation with hard magnets and hard metal coils serve as the backbone for most mechanical systems today.

To combine the benefits of both classical hard motors and deformation-based systems, we develop novel soft electromagnetic actuator concepts. These systems consist of liquid metal coils, compliant iron composites, and compliant permanent magnets. Some previous work has utilized liquid metal for electronics [15], [16], [17], sensing [18], [19], [20], [21], and attraction-based actuation [22], [23]. Actuation using traditional hard magnets [24], [25] and compliant permanent magnetic composites [26], [27], [28], [29] have also recently been studied. In this work, we combine liquid metal coils, compliant iron composites, and compliant permanent magnets for the first time to create stand-alone soft robotic actuators. Not only can this new topology be implemented for rotation, linear translation, attraction, and repulsion motions seen in traditional motors, but it can also be utilized to generate bending, contraction, and expansion motions seen in other soft actuators. Because forces on the compliant magnets can act at a distance, these actuators can also morph and move in other unique ways not seen in either hard electromagnetic actuators or in soft deformation-based actuators.

Compliant electromagnetic actuation also has another important potential benefit. Unlike electroactive polymers and some other soft actuators, compliant electromagnetic actuators can be designed to achieve the energy efficiencies, displacements, and bandwidths that approach those seen in traditional hard electromagnetic motors. Faster actuation speed further allows compliant electromagnetic actuators to take advantage of mechanical resonances for dynamic biologically-inspired motions.

In this work, we first demonstrate design concepts for liquid metal coils, followed by manufacturing methods for compliant magnets and iron composites. These new materials are characterized and co-fabricated to generate pulsing motions [5] inspired by the movement of soft corals from the genus *Xenia* [31]. The soft appendages of the coral (∼1 cm in length) pulsate to increase the flow of water, refresh the oxygen supply, and promote photosynthesis. To demonstrate some of the capabilities of this actuator topology, the motions of the *Xenia* coral appendages are translated to a compli-

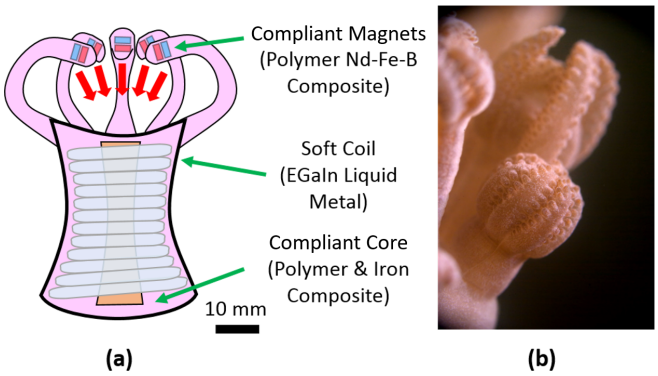


Fig. 1. (a) Exemplary soft robot constructed using compliant electromagnetic actuation concepts and (b) biological inspiration showing the pulsing/grasping motion of a *Xenia* coral [30] are exhibited.

* Corresponding Author

[1]N. Kohls, B. Dias, Y. Mensah, and Y. C. Mazumdar are with the School of Mechanical Engineering, Georgia Institute of Technology, Atlanta, GA 30332, USA, ellen.mazumdar@me.gatech.edu

[2]B. P. Ruddy is with the Auckland Bioengineering Institute, The University of Auckland, Auckland, 1010, New Zealand b.ruddy@auckland.ac.nz

ant electromagnetic actuation-based soft robot, as shown in Fig. 1. To maximize the displacement of the arms, the compliant electromagnetic actuators are driven at resonant frequencies. This attraction and repulsion-based actuation concept is then modelled and characterized to demonstrate how the dynamics and displacement scale with respect to actuator design choices.

## II. SOFT LIQUID METAL COILS

Liquid metal coils must have a conductor that is liquid at the operating temperature and a high conductivity to maximize output force and minimize resistive losses. Pure gallium metal has a melting point slightly above room temperature (29.8 °C) and has a relatively low resistivity ($1.36\times10^{-7}$ Ω·m) [32]. When this is combined with indium at a ratio of 3:1, a eutectic gallium-indium (EGaIn) alloy is created [33]. Although this eutectic has a slightly higher resistivity ($2.94\times10^{-7}$ Ω·m), it has a melting point below room temperature (15.5 °C), enabling the construction of liquid metal coils [33]. When compared with copper, the resistivity of EGaIn is 17.5 times higher. Lower melting temperatures can be achieved with Galinstan (mixture of gallium, indium, and tin), however, it was observed that the wetting properties of EGaIn made it easier to work with for soft coil applications.

Different encapsulation materials and manufacturing methods were considered, including molded flat electromagnetic spirals [23]. However, hollow thin-walled silicone tubing encapsulation was chosen due to the variety in available material hardnesses, high ductility (0.8 to 5.3 m/m) [34], and ability to form long conductor lengths into three-dimensional shapes. After EGaIn was injected into the tubing and wound around a bobbin, the resulting liquid metal coil was notably more flexible than hard copper coil counterparts and could withstand larger deformations and stretching. Each end of the coil was then attached to a small reservoir containing a small amount of additional liquid metal. Stainless steel electrodes were then inserted into the reservoir to make electrical contact. This electrical contact mechanism has several benefits. First, it provides hydrostatic pressure on the liquid metal inside the coil, thereby minimizing the introduction of bubbles. Second, excess pressure in the soft coils (due to compressive loads or thermal expansion) could be relieved or measured. Finally, because EGaIn forms passivating oxide layers when it comes in contact with oxygen, the reservoir prevents the formation of oxide inside the flexible coil and maintains high coil conductivity.

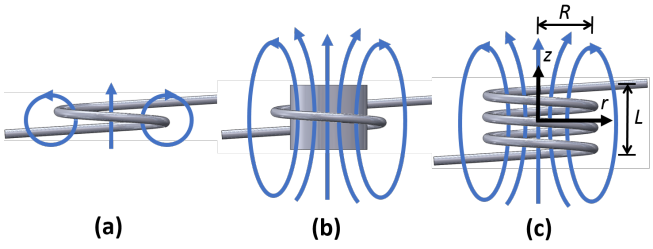


Fig. 2. (a) The magnetic field of a single loop of current carrying wire can be altered (b) by increasing the magnetic permeability with an iron core or (c) by increasing the number of turns in the wire.

The design principles for soft liquid metal coil geometries are similar to rigid copper coils, as illustrated in Fig. 2. For a coil formed into a solenoid, as illustrated in Fig. 2c, the magnetic flux density [35], [36] in the $r$ and $z$ directions from the center of the coil can be calculated as,

$$\vec{B_s} = B_r(r,z)\hat{r} + B_z(r,z)\hat{z}, \tag{1}$$

such that,

$$B_r = \frac{\mu n I}{\pi}\left[\alpha_+ E(\delta_+,1,1,-1) - \alpha_- E(\delta_-,1,1,-1)\right], \tag{2}$$

$$B_z = \frac{\mu n I R}{\pi(R+r)}\left[\beta_+ E(\delta_+,\gamma^2,1,\gamma) - \beta_- E(\delta_-,\gamma^2,1,\gamma)\right], \tag{3}$$

where $R$ is the radius of the coil, $L$ is the height of the coil, $z_\pm = z \pm L/2$, and,

$$\alpha_\pm = \frac{R}{\sqrt{z_\pm^2 + (r+R)^2}}, \tag{4}$$

$$\beta_\pm = \frac{z_\pm}{\sqrt{z_\pm^2 + (r+R)^2}}, \tag{5}$$

$$\gamma = \frac{R-r}{R+r}, \tag{6}$$

$$\delta = \sqrt{\frac{z_\pm^2 + (R-r)}{z_\pm^2 + (R+r)^2}}. \tag{7}$$

Here, the elliptical integrals are represented by,

$$E(k,p,c,s) = \int_0^{\pi/2} \frac{(c\cos^2\theta + \sin^2\theta)d\theta}{(\cos^2\theta + p\sin^2\theta)\sqrt{\cos^2\theta k^2 + \sin^2\theta}}. \tag{8}$$

From these equations, it is clear that increasing the current $I$, magnetic permeablity $\mu$, and the number of turns $n$ can all increase the overall magnetic field strength generated by the coil. The coil resistance $Z$ can be calculated using $Z = \rho n R^2/a^2$ where $a$ is the radius of the liquid metal encapsulation tube. Design trade-offs between coil resistance, coil dimensions, and coil magnetic field can then be made using these equations.

## III. COMPLIANT MAGNETIC & IRON COMPOSITES

In soft electromagnetic actuators, compliant iron and permanent magnetic composites are needed to improve the magnetic permeability of coils and to generate magnetic fields without using electrical power. Inspired by traditional hard iron cores and hard rare-earth magnets, new compliant composites were created by combining iron and rare-earth powders with two-part silicone polymers. The combined material inherits compliance properties from the polymer and magnetic properties from the metal powders. The primary trade-offs between compliant versus smaller hard magnets with the same field strength are deformability, size, and the ability to customize the structure of the magnetic field. Concepts for material processing were iterated quickly using

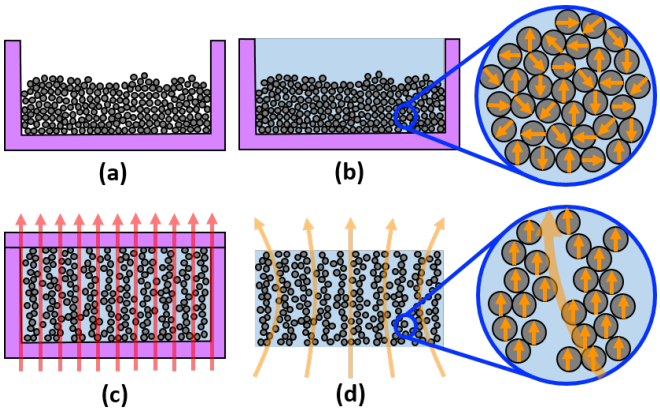


Fig. 3. The manufacturing process for compliant permanent magnets and compliant iron composites is illustrated. (a) Particles are placed into mold and then (b) mixed with a silicone polymer. (c) The magnetic poles of the composite are then oriented with a strong external magnetic field, which, when removed after curing, (d) leaves a soft composite with a weaker residual magnetic field.

molds created via additive manufacturing. The final manufacturing process, which produced the strongest and most uniform compliant magnets and iron cores, is shown in Fig. 3.

In this process, iron or pre-magnetized rare earth magnetic powders are first placed inside a mold and mixed thoroughly with silicone polymer. While finer powders stay suspended in the mixture, coarser powders tend to settle during curing. In addition, as shown in Fig. 3b, magnetic particles tend to attract, producing composites with randomly oriented poles and weak magnetic fields. To align the poles inside the polymer and to distribute particles more evenly throughout the height of the mold during curing, a cap is placed on the mold and a strong external magnetic field is applied. Field strengths of 0.45 T (4500 G) or more can be generated with large permanent magnets placed both above and below the mold. With the application of an external magnetic field, the particles line up into strands, filling the mold. When the external magnetic field is removed, as shown in Fig. 3d, the cured composite material retains a residual magnetic field from the oriented particles.

### A. Compliant Magnetic Composites

Unlike magnetization processes for hard magnets, which reorient the magnetic field of microdomains inside the solid, this process operates at lower field strengths and primarily rotates particles with pre-existing magnetic fields. Therefore pre-magnetized particles are required for creating compliant magnetic materials. To optimize the properties of strong permanent magnetic polymers, pre-magnetized Nd-Fe-B powders were combined with silicone of varying hardness (EcoFlex 10, 20, 30, and 50 with numbers corresponding to the Shore OO durometer). Magnets manufactured with EcoFlex 10 were found to fall apart after removal from the mold because the cured polymer could not withstand the strong residual internal magnetic forces produced by the oriented magnetic powders. As the Shore hardness increased, the percentage of magnetic powder (by mass) that could be added to the composite also increased. Ultimately, EcoFlex

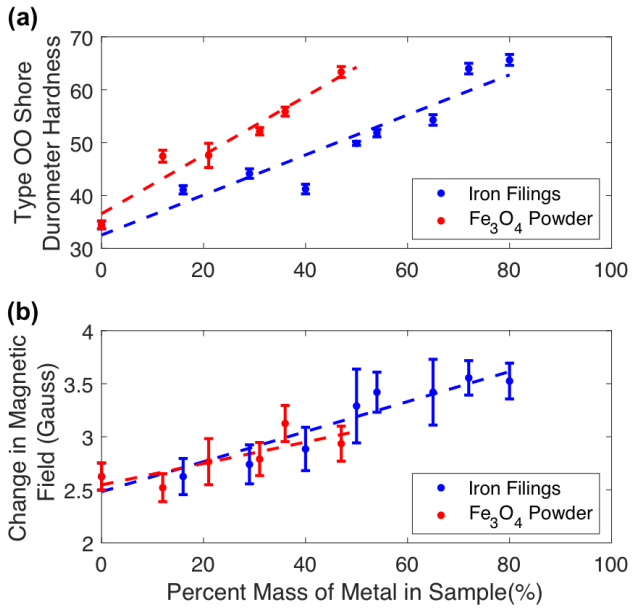


Fig. 4. (a) The type OO Shore durometer hardness and (b) the change in magnetic field strength when placed inside an electomagnetic coil are shown as a function of percent mass of either iron filings or $Fe_3O_4$ mixed with silicone. Change in the magnetic field was measured after applying 1 A to an electromagnetic copper coil (diameter D = 17 mm, height H = 7 mm, n = 7 turns, and 20 AWG gauge wire).

50 was found to produce the strongest compliant permanent magnets with the highest proportion of Nd-Fe-B powder at 77% by mass. For a 1.23 g compliant magnet, the maximum surface magnetic field is 0.065 T (650 G), which is strong enough to lift its own weight and stick to steel surfaces.

### B. Compliant Iron Composites

Hard iron cores are often added to hard solenoids to increase the magnetic permeability and enhance the magnetic field output. To tune the properties of compliant iron cores, two iron powders were tested, one with larger iron filing particles (diameters up to 300 $\mu$m) and a second with smaller $Fe_3O_4$ powder (diameters up to 100 nm). While $Fe_3O_4$ powder is finer and suspends well inside silicone during curing, iron filing powders are larger. Therefore, they require an externally applied magnetic field during manufacturing to prevent settling and to create a more uniform magnetic field. However, because the residual magnetic forces in compliant iron composites are significantly lower than the residual forces in compliant permanent magnet composites, the silicone durometer (and overall composite hardness) can be chosen independently from the magnetic permeability properties.

Figure 4a shows how the hardness of the composite varies as the percent mass of metal is increased up to saturation (after which the silicone no longer polymerizes). For iron, saturation occurred near 80% by mass and for $Fe_3O_4$ saturation occurred near 50% by mass. Results indicate that the hardness of the composites made with iron filings is lower than that of the corresponding $Fe_3O_4$ samples with the same percent mass of metal. In addition, the maximum hardness

achieved prior to saturation for both powders is the same, at approximately 70. Based on the results, we believe that these effects are due to the particle sizes. Because $Fe_3O_4$ powders are finer with a larger surface-area-to-volume ratio, they require more silicone to fully surround the particles. Therefore, the iron filings composites can be loaded at a higher percentage by weight before saturation.

To assess the magnetic permeability, each compliant iron sample was placed at the center of a coil. A current was applied to the coil and the magnetic field at the top of the coil was then measured using a gaussmeter. The resulting change in magnetic field strength, which corresponds to the magnetic permeability, is shown in Fig. 4b. Here, the change in magnetic field for both powders is approximately the same for the same percent mass. This indicates that the permeability of the two powders is similar. Because the iron filing samples were able to achieve higher concentrations before saturation, they were therefore the best candidates for the ferromagnetic cores.

## IV. SOFT ATTRACTION & REPULSION ACTUATOR INSPIRED BY **XENIA** CORAL

Soft coils, compliant permanent magnets, and compliant iron composites can be combined to create a fully soft robotic actuator. For this work, a soft attraction/repulsion actuator was created to simulate the motion of a *Xenia* coral, as illustrated in Fig. 5. First, an iron-filing composite core (80% by weight iron filings mixed with Ecoflex 50, 10 mm diameter) was molded and attached to polymer disks to create a bobbin (32 mm tall, 38 mm diameter). Next, EGaIn was injected into a silicone tube (1 mm inner diameter, 2 mm outer diameter, 5 m length) and wound (n = 70) around the bobbin. The resulting resistance of the coil was 2.2 Ω.

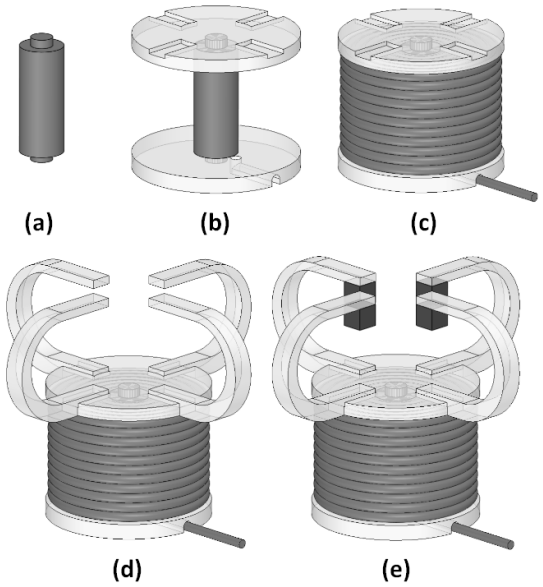


Fig. 5. The fabrication process of the *Xenia* coral soft robot is shown. (a) An iron-silicone composite is molded and (b) attached to two silicone polymer disks. (c) Liquid EGaIn-filled tubing is wound around the core and (d) compliant silicone arms are attached at the top. (e) Finally, compliant permanent magnets are attached to the tip of each arm.

After the coil was constructed, the stiffness and total stroke of soft arms were tuned by adjusting the arm geometry, mixing different proportions of Ecoflex silicone with Polydimethylsiloxane (PDMS), and optimizing the mass of the compliant permanent magnets. Reducing the stiffness of the arms or increasing the volume of the magnets results in a longer stroke. However, if the arm stiffness is too low to support the weight of the magnet, the arms will fold downward. Additionally, if the arms are too long or if the magnets are too strong, the compliant arms will attract. After several design iterations, a 1:1 ratio of Ecoflex-50 and PDMS was combined to build the arms. Each arm was joined with a single 0.15 g compliant magnet (77% by mass Nd-Fe-B powder mixed with Ecoflex-50), oriented to maximize the arm stroke.

The model and prototype of the final *Xenia*-inspired actuator are illustrated in Fig. 6. When current is applied to the liquid metal coil, an electromagnetic field is generated and enhanced by the compliant iron composite core. The field generated by the coil, described in Eq.(2) and (3), interacts with the magnetic fields generated by the compliant magnets, resulting in attraction and repulsion motions, which bend the soft arms.

Each compliant magnet can be approximated using a simple dipole model,

$$\vec{B}_d = \frac{\mu_m M_0 V}{4\pi}\left(\frac{3(\vec{m}\cdot\vec{x})\vec{x}}{\|\vec{x}\|^5} - \frac{\vec{m}}{\|\vec{x}\|^3}\right), \tag{9}$$

where $\mu_m$ is the permeability of the magnetic material, $M_0$ is the uniform magnetization, $V$ is the volume, $\vec{m}$ is the magnetic moment, $\vec{x}$ is the position vector, and $\|\cdot\|$ is the $L_2$ norm. The magnetic moment is normalized such that $\|\vec{m}\| = 1$. The force that the coil exerts [37] on a single compliant magnet is complex but can be modeled as,

$$\vec{F} = M_0 V \nabla(\vec{B}_s \cdot \vec{m}). \tag{10}$$

The force exerted on the compliant magnet is nonlinear and is stronger near the coil during attraction and weaker further away from the coil during repulsion.

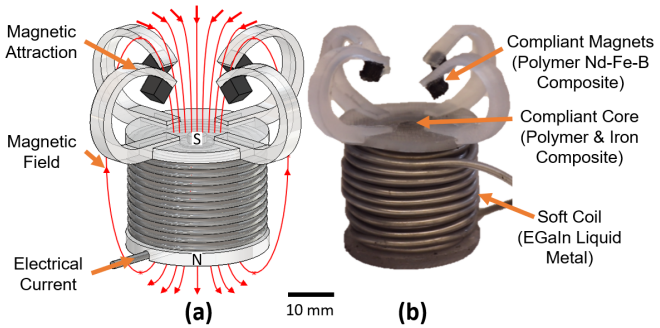


Fig. 6. Motion for the compliant electromagnetic actuator is generated when the permanent magnetic tips are attracted towards or repelled by the applied electromagnetic field. The (a) model and (b) prototype for a biologically-inspired *Xenia* coral are illustrated.

## V. EXPERIMENTAL RESULTS & CHARACTERIZATION

To operate the soft actuator, a microcontroller is used to drive a Pololu G2 18v25 high-power motor driver (30 V and 25 A max) using pulse width modulation (PWM) signals. To verify the displacement of each arm, a Phantom VEO-E 310L color high speed camera was utilized. A timing signal generated with the microcontroller was used as an input trigger for each frame captured by the high speed camera in order to synchronize the input command with the measured video frames. The location of compliant magnets were then tracked using custom software in MATLAB.

Figure 7(a) shows the relationship between the supply current and the vertical $y$-displacement of the magnet. A second-order polynomial was then fit to the data. The vertical displacement is nonlinear, as predicted by the force model in Eq.(10). When supplied at 5 A, the displacement was more than 2 mm during attraction and only slightly more than 1 mm during repulsion. Due to the design of the bending arms, a small amount of out-of-plane motion in the $x$-direction was also detected. For this operating range, there was no noticeable effect of power dissipation and device temperature on performance.

After inverting the nonlinear map, a simple small-displacement motion profile similar to the pulsing motion of the *Xenia* coral arms was created. The desired planned path and measured path are shown in Fig. 7b. Although no sensor feedback was used for this experiment, the magnetic tip was able to accurately follow the planned path. Small oscillations at the natural frequency of the silicone/PDMS arms are noted in the motion profile. These oscillations are associated with the low damping of the arms while operating in an air environment.

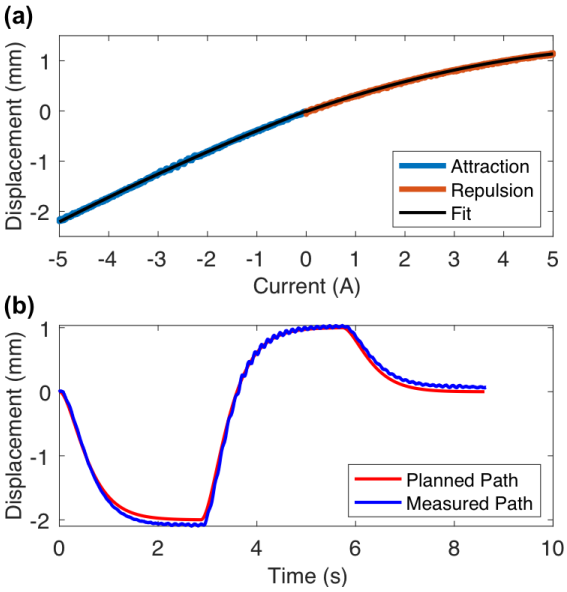


Fig. 7. (a) The nonlinear vertical $y$-displacement of a compliant magnetic tip as a function of steady-state input current is illustrated. The attraction and repulsion curves are fit with a second-order polynomial. (b) The desired and measured trajectories (after accounting for the nonlinear relationship) for a single soft arm with a compliant magnetic tip are shown.

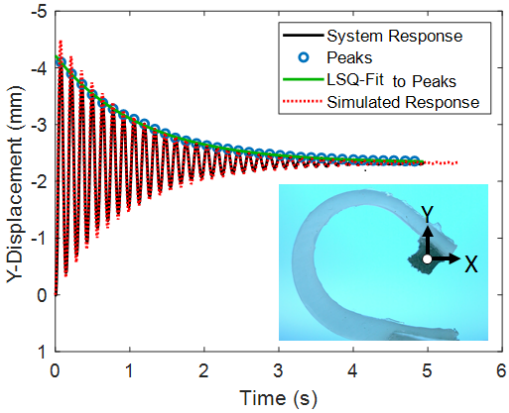


Fig. 8. Magnitude of the step response in the y-direction during attraction is illustrated for a single soft arm with a compliant magnetic tip (image inset). The peaks of the oscillatory response were fit to an exponential decay function and the natural frequency and damping ratio were calculated to create a linear simulated response. Differences in the envelope of the physical and simulated responses suggest nonlinear effects.

To better characterize the dynamics, step responses of individual arms with compliant magnetic tip were obtained, as illustrated in Fig. 8. An attraction step response with a steady-state input of 5 A and 11 V was obtained and the magnitude of the $y$-displacement was tracked from high speed camera data. Approximating the response as second-order, the envelope oscillations were identified by using the peaks of the response to generate a least-squares fit. Next, a simulated second-order response was generated to fit to the measured system response. Because of the low damping in the flexible arms, the total motion is on the order of 4 mm even though the steady-state displacement is only 2 mm.

After conducting several step response experiments, the natural frequency of the system was determined to be between 6.5 and 7.5 Hz and the damping ratio was determined to be between 0.03 and 0.09. This translates to a gain of 0.21 mm/V, an effective mass of 0.31 g, an effective soft arm stiffness of 0.62 N/m, and a damping of 0.63 mN·s/m. When the simulated linear response was compared to the measured step response, it is clear that the envelopes do not match perfectly, which also implies that the system is nonlinear.

To identify the high-frequency system response, stochastic system identification techniques were used [38], [39]. In this technique, a pseudo-random binary signal is input to the system and the motion of a single compliant magnet was measured. A short snippet of the input and output are illustrated in Fig. 9a. The transfer function estimate of the magnitude and phase is shown in Fig. 9b and c. As predicted by the step response, the natural frequency of the actuator is measured to be around 7 Hz with a 180 degree phase shift, indicating a dominant second-order response. As the frequency of the input increases, additional peaks corresponding to structural resonances in the soft arms can also be observed. In addition, the signal to noise ratio also decreases at higher frequencies. The magnitude-squared coherence (MSC) of the input/output relationship, as shown in Fig. 9d, represents an estimate of the proportion of the signal at each frequency that can be modeled as linear.

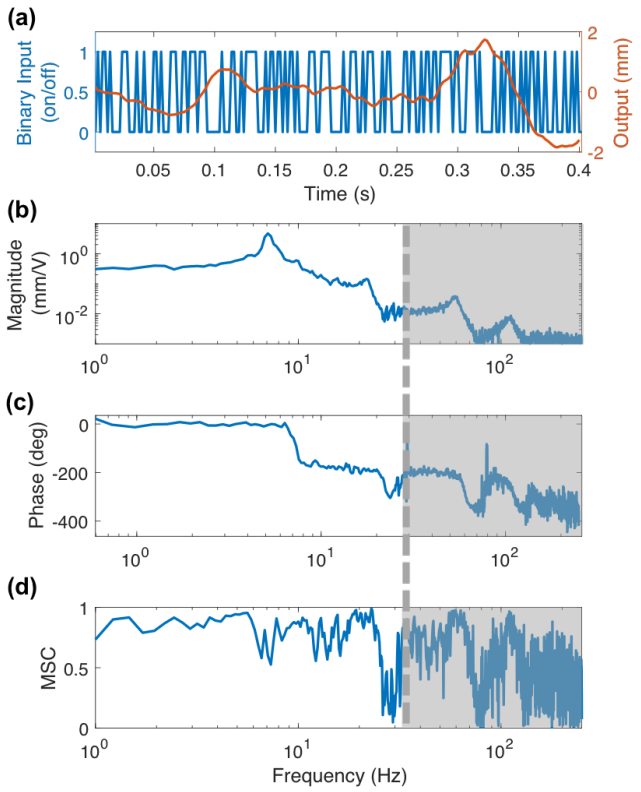


Fig. 9. The frequency response gathered using the stochastic system identification technique shows the (a) input & output, (b) magnitude, (c) phase, and (d) magnitude-squared coherence (MSC) of a single soft arm with a compliant magnetic tip moving in the *y*-direction. This data was recorded at 500 fps with 8000 samples. The gray area indicates portions with lower signal-to-noise and higher uncertainty.

Driving the *Xenia*-inspired robot with multiple compliant arms at resonance produces larger arm motions, as illustrated in Fig. 10. A video included with this paper demonstrates the motion of the *Xenia* arms driven at low frequencies and at high resonant frequencies. Because each compliant arm has a slightly different mass and stiffness, the motion of the arms eventually moves slightly out of synchronization. The natural frequency of this robot can be increased by either decreasing the effective mass of the arms and compliant magnets or by increasing the stiffness via tuning the geometry or the material properties of the arms. By placing the compliant magnets closer to the center of the coil, the efficiency of the robotic actuator can also be improved.

## VI. CONCLUSION

In this work, a new compliant actuation concept was developed using liquid metal coils, compliant iron cores, and compliant permanent magnets. The scaling laws and manufacturing methods for the novel composite materials was then discussed. The new electromagnetic actuator concept is capable of both traditional hard electromagnetic actuator motions (such as linear translation, rotation, attraction and repulsion) and soft compliant actuator motions (such as bending, compression, expansion). Thus, an exemplary soft robot was created from different compliant electromagnetic actuator elements to simulate the pulsing motions of a

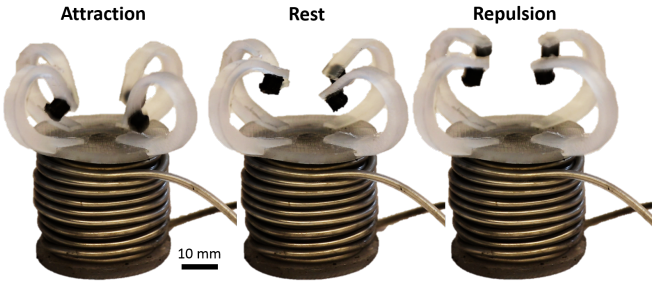


Fig. 10. Attraction, rest, and repulsion configurations of the soft electromagnetic *Xenia*-inspired actuator when operated at the resonant frequency of 7 Hz. A video included with this paper demonstrates the motion of the arms.

*Xenia* coral. Taking advantage of the attraction and repulsion actuation concepts, the resulting soft robot was characterized and then used to perform pre-planned low frequency motions that ranged from -2 mm to 1 mm (with $\pm$5 A and $\pm$11 V input) in steady state. The resonant response of the soft arms was also utilized to generate larger displacements of -4 mm to 2 mm (limited to $\pm$11 V input).

The strong resonant frequency and nonlinearity in motion introduce interesting challenges for closed loop control. To further increase the nonlinear actuator stroke, different actuator configurations can be investigated. To decrease the strong resonant frequency, additional damping can be introduced. One reason for the weaker resonant frequency in real *Xenia* coral is that they operate under water, where the viscosity introduces additional damping. Indeed, when the soft robot was placed under water, higher damping was noted. One possible future solution for air-operation is to increase the damping by redesigning material and geometry of the soft arms. Another possible solution is to introduce feedback control with a soft position, orientation, or bend sensors [40], [41], [42], [20], [43]. Soft actuation techniques can also be effectively combined with complementary sensing techniques to measure shear [44], force [45], and temperature [46], [47].

Overall, this work creates an interesting starting point for future development of compliant electromagnetic actuators. The current actuator could be used to help circulate fluid. However, soft electromagnetic actuators could be used in the future for grasping and completing other complex continuum motions. With future advancements in design and manufacturing of soft liquid coils, compliant iron composites, and compliant permanent magnets, new mechanisms and actuation topologies can also be developed. This will enable a suite of new soft robots with performance and efficiencies that begin to approach conventional hard actuators.

## ACKNOWLEDGMENT

The authors would like to thank the Georgia Tech Institute for Robotics and Intelligent Machines for their support, Dr. Frank Dellaert and Mandy Xie for their collaboration, and the Dynamic Adaptive Robotic Technologies (DART) laboratory for assistance with equipment.

## REFERENCES


[1] H. Zeng, O. M. Wani, P. Wasylczyk, and A. Priimagi, "Light-driven, caterpillar-inspired miniature inching robot," *Macromolecular Rapid Communications*, vol. 39, p. 1700224, 2017.

[2] C. Yuan, D. J. Roach, C. K. Dunn, Q. Mu, X. Kuang, C. M. Yakacki, T. J. Wang, K. Yu, and H. J. Qi, "3D printed reversible shape changing soft actuators assisted by liquid crystal elastomers," *Soft Matter*, vol. 13, pp. 5558–5568, 2017.

[3] H. Jin, E. Dong, M. Xu, C. Liu, G. Alici, and Y. Jie, "Soft and smart modular structures actuated by shape memory alloy (SMA) wires as tentacles of soft robots," *Smart Materials and Structures*, vol. 25, p. 085026, 2016.

[4] R. Z. Pytel, E. L. Thomas, Y. Chen, and I. W. Hunter, "Anisotropic actuation of mechanically textured polypyrrole films," *Polymer*, vol. 49, no. 5, pp. 1338–1349, 2008.

[5] M. Otake, M. Inaba, and H. Inoue, "Development of a gel robot made of electro-active polymer PAMPS gel," in *IEEE International Conference on Systems, Man, and Cybernetics*, 1999, pp. 788–793.

[6] J. J. Shintake, S. S. Rosset, B. D. F. B. Schubert, and H. Shea, "Versatile soft grippers with intrinsic electroadhesion based on multifunctional polymer actuators," *Advanced Materials*, vol. 28, pp. 231–238, 2016.

[7] C. Cvetkovic, R. Raman, V. Chan, B. J. Williams, M. Tolish, P. Bajaj, M. S. Sakar, H. H. Asada, M. T. A. Saif, and R. Bashir, "Three-dimensionally printed biological machines powered by skeletal muscle," *Proceedings of the National Academy of Sciences*, vol. 111, pp. 10 125–10 130, 2014.

[8] F. Fries, S. Miyashita, D. Rus, R. Pfeifer, and D. D. Damian, "Electromagnetically driven elastic actuator," in *IEEE International Conference on Robotics and Bioimimetrics (ROBIO)*, 2014, pp. 309–314.

[9] M. Wehner, R. L. Truby, D. J. Fitzgerald, B. Mosadegh, G. M. Whitesides, J. A. Lewis, and R. J. Wood, "An integrated design and fabrication strategy for entirely soft, autonomous robots," *Nature*, vol. 536, pp. 451–455, 2016.

[10] R. K. Katzschmann, A. D. Marchese, and D. Rus, "Hydraulic autonomous soft robotic fish for 3D swimming," *Experimental Robotics*, vol. 109, pp. 405–420, 2016.

[11] F. Ilievski, A. D. Mazzeo, R. F. Shepherd, X. Chen, and G. M. Whitesides, "Soft robotics: a bioinspired evolution in robotics," *Angewandte Chemie International Edition*, vol. 50, no. 8, pp. 1890–1895, 2011.

[12] S. I. Rich, R. J. Wood, and C. Majidi, "Untethered soft robotics," *Nature Electronics*, vol. 1, pp. 102–112, 2018.

[13] D. Rus and M. T. Tolley, "Design, fabrication and control of soft robots," *Nature*, vol. 521, pp. 467–475, 2015.

[14] S. Kim, C. Laschi, and B. Trimmer, "Soft robotics: a bioinspired evolution in robotics," *Trends in Biotechnology*, vol. 31, no. 7, pp. 287–294, 2013.

[15] C. Wang, C. Wang, Z. Huang, and S. Xu, "Materials and structures towards soft electronics," *Advanced Materials*, vol. 30, p. 1801368, 2018.

[16] R. Guo, X. Sun, S. Yao, M. Duan, H. Wang, J. Liu, and Z. Deng, "Semi-liquid-metal-(Ni-EGaIn)-based ultraconformable electronic tattoo," *Advanced Materials Technologies*, vol. 4, 2019.

[17] S. Zhu, J. So, R. Mays, S. Desai, W. R. Barnes, B. Pourdeyhimi, and M. D. Dickey, "Ultrastretchable fibers with metallic conductivity using a liquid metal alloy core," *Advanced Functional Materials*, vol. 23, pp. 2308–2314, 2013.

[18] M. D. Dickey, "Stretchable and soft electronics using liquid metals," *Advanced Materials*, vol. 29, p. 1606425, 2017.

[19] Y.-L. Park, B.-R. Chen, and R. J. Wood, "Design and fabrication of soft artificial skin using embedded microchannels and liquid conductors," *IEEE Sensors Journal*, vol. 12, no. 8, pp. 2711–2718, 2012.

[20] J.-P. Chossat, Y.-L. Park, R. J. Wood, and V. Duchaine, "Soft strain sensor based on ionic and metal liquids," *IEEE Sensors Journal*, vol. 13, no. 9, pp. 3405–3414, 2013.

[21] M. A. Robertson, L. Dejace, S. P. Lacour, and J. Paik, "Bi-modal control of vacuum-powered soft pneumatic actuators with embedded liquid metal-based strain sensitive skin," in *IEEE International Conference on Soft Robotics (RoboSoft)*, 2019, pp. 217–221.

[22] S. W. Jin, J. Park, S. Y. Hong, H. Park, Y. R. Jeong, S.-S. L. J. Park, and J. S. Ha, "Stetchable loudspeaker using liquid metal microchannel," *Nature Scientific Reports*, vol. 5, p. 11695, 2015.

[23] R. Guo, L. Sheng, H.-Y. Gong, and J. Liu, "Liquid metal spiral coil enabled soft electromagnetic actuator," *Science China*, vol. 61, no. 4, pp. 516–521, 2018.

[24] J. Berengueres, K. Tadakuma, T. Kamoi, and R. Krat, "Compliant distributed magnetic adhesion device for wall climbing," in *IEEE International Conference on Robotics and Automation*, 2013, pp. 1256–1261.

[25] J. J. Abbott, O. Ergeneman, M. P. Kummer, A. M. Hirt, and B. J. Nelson, "Modeling magnetic torque and force for controlled manipulation of soft-magnetic bodies," *IEEE Transactions on Robotics*, vol. 23, no. 6, pp. 1247–1252, 2007.

[26] R. Zhao, Y. Kim, S. A. Chester, P. Sharma, and X. Zhao, "Mechanics of hard-magnetic soft materials," *Journal of the Mechanics and Physics of Solids*, vol. 124, pp. 244–263, 2019.

[27] Y. Kim, H. Yuk, R. Zhao, S. A. Chester, and X. Zhao, "Printing ferromagnetic domains for untethered fast-transforming soft materials," *Nature*, vol. 558, pp. 274–279, 2018.

[28] Y. Kim, G. A. Parada, S. Liu, and X. Zhao, "Ferromagnetic soft continuum robots," *Science Robotics*, vol. 4, 2019.

[29] T. N. Do, H. Phan, T.-Q. Nguyen, and Y. Viseli, "Miniature soft electromagnetic actuators for robotic applications," *Advanced Functional Materials*, vol. 28, no. 18, p. 1800244, 2018.

[30] Nebarnix, "Coral closeup," Available at https://search.creativecommons.org/photos/dc9793de-3ab2-445f-8ecc-8e82a8e3e1a4, licensed under CC BY 2.0.

[31] M. Kremien, U. Shavit, T. Mass, and A. Genin, "Benefit of pulsation in soft corals," *Proceedings of the National Academy of Sciences*, vol. 110, no. 22, pp. 8978–8983, 2013.

[32] D. R. Lide, *CRC Handbook of Chemistry and Physics*. Boca Raton, FL: CRC Press, 2005.

[33] M. D. D. et al, "Eutectic gallium-indium (EGaIn): A liquid metal alloy for the formation of stable structures in microchannels at room temperature," *Advanced Functional Materials*, vol. 18, p. 10971104, 2008.

[34] AZOMaterials, "Silicone rubber," Available at https://www.azom.com/properties.aspx?ArticleID=920 (2019).

[35] N. Derby and S. Olbert, "Cylindrical magnets and ideal solenoids," *American Journal of Physics*, vol. 78, no. 19, pp. 229–235, 2010.

[36] A. Caciagli, R. J. Baars, A. P. Philipse, and B. W. Kuipers, "Exact expression for the magnetic field of a finite cylinder with arbitrary uniform magnetization," *Journal of Magnetism and Magnetic Materials*, vol. 456, pp. 423–432, 2018.

[37] W. Robertson, B. Cazzolato, and A. Zander, "Axial force between a thick coil and a cylindrical permanent magnet: Optimizing the geometry of an electromagnetic actuator," *IEEE Transactions on Magnetics*, vol. 48, no. 9, pp. 2479–2487, 2012.

[38] B. Peeters and G. De Roecks, "Stochastic system identification for operational modal analysis: A review," *Journal of Dynamic Systems, Measurement, and Control*, vol. 123, no. 4, pp. 659–667, 2001.

[39] Y. Chen and I. W. Hunter, "Stochastic system identification of skin properties: Linear and Wiener static nonlinear methods," *Annals of Biomedical Engineering*, vol. 40, no. 10, pp. 2277–2291, 2012.

[40] Y. Chen, J. M. Oliveira, and I. W. Hunter, "Two-axis bend sensor design, kinematics and control for a continuum robotic endoscope," in *IEEE International Conference on Robotics and Automation (ICRA)*, 2013, pp. 696–702.

[41] Y. Chen, J. M. Oliveira, and I. W. Hunter, "Sensor architecture for a two-actuator robotic endoscope tip," in *International Conference of the IEEE Engineering in Medicine and Biology Society*, 2011, pp. 8340–8343.

[42] L. Viry, A. Levi, M. Totaro, A. Mondini, V. Mattoli, B. Mazzolai, and L. Beccai, "Flexible three-axis force sensor for soft and highly

sensitive artificial touch," *Advanced Materials*, vol. 26, pp. 2659–2664, 2014.

[43] Y. Chen, A. Mazumdar, C. F. Brooks, B. G. van Bloemen Waanders, S. D. Bond, and M. B. Nemer, "Remote distributed vibration sensing through opaque media using permanent magnets," *IEEE Transactions on Magnetics*, vol. 54, no. 6, pp. 1–13, 2018.

[44] P. Roberts, D. D. Damian, W. Shan, T. Lu, and C. Majidi, "Soft-matter capacitive sensor for measuring shear and pressure deformation," in *IEEE International Conference on Robotics and Automation*, 2013, pp. 3529–3534.

[45] D. M. Vogt, Y.-L. Park, and R. J. Wood, "Design and characterization of a soft multi-axis force sensor using embedded microfluidic channels," *Annals of Biomedical Engineering*, vol. 13, no. 10, pp. 4056–4064, 2013.

[46] Y. Chen, O. Guba, C. F. Brooks, C. C. Roberts, B. G. van Bloemen Waanders, and M. B. Nemer, "Remote temperature distribution sensing using permanent magnets," *IEEE Transactions on Magnetics*, vol. 53, no. 2, pp. 1–13, 2017, 6000113.

[47] A. Mazumdar, Y. Chen, B. G. van Bloemen Waanders, C. F. Brooks, M. Kuehl, and M. B. Nemer, "Wireless temperature sensing using permanent magnets for nonlinear feedback control of exothermic polymers," *IEEE Sensors Journal*, vol. 18, no. 19, pp. 7970–7979, 2018.